Journal of Power Sources 260 (2014) 259–263

Contents lists available at ScienceDirect

Journal of Power Sources

journal homepage: www.elsevier.com/locate/jpowsour

Short communication

Reduced-temperature firing of solid oxide fuel cells with zirconia/ceria bi-layer electrolytes

Zhan Gao*, David Kennouche, Scott A. Barnett

Department of Materials Science and Engineering, Northwestern University, 2220 Campus Drive, Evanston, IL 60208, USA

HIGHLIGHTS

- Dense bi-layer zirconia/ceria electrolytes have been co-fired at 1250 °C for SOFC.
- YSZ/GDC interdiffusion and Sr diffusion through the GDC layer were minimized.
- High electrochemical activity Ni–YSZ anode with high TPB densities is obtained.

ARTICLE INFO

Article history:
Received 8 January 2014
Received in revised form
27 February 2014
Accepted 5 March 2014
Available online 19 March 2014

Keywords:
Solid oxide fuel cell
Bi-layer electrolyte
Reduced-temperature firing
Sintering aid
Interdiffusion

ABSTRACT

Solid oxide fuel cells (SOFCs) with bi-layer Zirconia/Ceria electrolytes have been studied extensively because of their great potential for producing high power density at reduced operating temperature, important for reducing cost and thereby allowing broader SOFC commercialization. The bi-layer electrolytes are designed to take advantage of the high oxygen ion conductivity of Ceria, the low electronic conductivity of Zirconia, and the low reactivity of Ceria with high-performance cathodes. However, zirconia/ceria processing has proven problematic due to interdiffusion during high temperature co-firing, or ceria layer porosity after two-step firing. Here we first show a new method for bi-layer co-firing at a reduced temperature of 1250 °C, ~150 °C lower than the usual sintering temperature, achieved using Fe_2O_3 as a sintering aid. This novel process enables high power density SOFCs by producing: (1) low-resistance $Y_{0.16}Zr_{0.92}O_{2-\delta}$ (YSZ)/$Gd_{0.1}Ce_{0.9}O_{1.95}$ (GDC) electrolytes that also yield high open-circuit voltage, (2) dense GDC layers that prevent reactions between highly-active $La_{0.6}Sr_{0.4}Fe_{0.8}Co_{0.2}O_3$ (LSFC) cathode materials and YSZ, and (3) Ni–YSZ anodes with high electrochemical activity due to fine-scale microstructure with high TPB densities.

1. Introduction

Bi-layer zirconia/ceria electrolytes are important for improving performance of solid oxide fuel cells (SOFCs). For example, ceria is widely used as a diffusion barrier layer to avoid reactions between high-performance electrode materials such as $La_{0.6}Sr_{0.4}Fe_{0.8}Co_{0.2}O_3$ (LSFC) and zirconia [1], and can also provide faster electrochemical kinetics than zirconia with some electrode materials [2–4]. The application to next-generation intermediate-temperature (≤600 °C) SOFCs, which are expected to have broader commercial applications than current (750–800 °C) SOFCs [5], is especially compelling. Although most intermediate-temperature SOFCs have employed high-conductivity single-layer ceria electrolytes [6], they generally yield low open-circuit voltage (OCV) [7]. The addition of a thin fuel-side stabilized-zirconia layer is useful for achieving near-theoretical OCV, but processing presents significant challenges; when fired together at temperatures typically used to form dense electrolytes, ~1400 °C, high electrolyte resistance results due to formation of a low conductivity zirconia/ceria interdiffused interfacial layer [8–12]. Here we show a method for obtaining yttria-stabilized zirconia (YSZ)/$Gd_{0.1}Ce_{0.9}O_{1.95}$ (GDC) bi-layers with minimal interdiffusion, enabled by a novel method for reducing the firing temperature to 1250 °C. The method is demonstrated in Ni–$Y_{0.16}Zr_{0.92}O_{2-\delta}$ (YSZ)/YSZ/$Gd_{0.1}Ce_{0.9}O_{1.95}$ (GDC)/$La_{0.6}Sr_{0.4}Fe_{0.8}Co_{0.2}O_3$ (LSFC)-GDC cells. The reduced firing temperature also yields a finer-scale Ni–YSZ microstructure, and the dense GDC barrier layer minimizes LSCF-YSZ reactions, both of which contribute to excellent cell performance: area-specific resistance as low as 0.21 Ω cm^2 and power density as high as 1.65 W cm^{-2} at 800 °C in air and humidified hydrogen.

* Corresponding author. Tel.: +1 8474912447; fax: +1 8474917820.
E-mail addresses: zhan.gao@northwestern.edu, zhangao.nu@gmail.com (Z. Gao).

http://dx.doi.org/10.1016/j.jpowsour.2014.03.025
0378-7753/

A successful SOFC fabrication process must avoid materials interactions and yield desired microstructures, but it is also important to minimize process cost and complexity. In the case of zirconia/ceria electrolyte cells, a few different process schemes have been employed:

(1) The anode and both electrolyte layers are co-fired at 1400 °C, followed by cathode application and firing [11]. This scheme minimizes process steps but is problematic due to interdiffusion, as noted above.
(2) The anode and YSZ electrolyte are co-fired at 1400 °C, followed by separate ceria deposition and firing steps, finally followed by the cathode. This approach is often used with LSFC-based cathodes, where the ceria is needed as a barrier layer to prevent LSCF/zirconia reactions that form the highly resistive zirconate phases $La_2Zr_2O_7$ and $SrZrO_3$ [13–15]. Since the thin ceria layer is fired at a temperature of ~1200 °C and the substrate is non-shrinking, the ceria has considerable porosity allowing non-negligible LSCF-zirconia reaction [16].
(3) An approach similar to (2), but utilizing physical vapor deposition to deposit the ceria layer, has been utilized. This has the advantage of producing dense ceria layers without high-temperature firing, but is a relatively expensive additional process step [3,4,7,9,17].

The present method is similar to case (1), in that it employs a single co-firing step for the anode and both electrolyte layers, but at a reduced co-firing temperature of 1250 °C. This has the advantages of a relatively simple process, but also minimizes zirconia/ceria interdiffusion. The main challenge is to produce sufficiently-dense electrolyte layers in a 1250 °C firing step; this has been achieved by including 1 mol.% Fe_2O_3 sintering-aid impurity in the ceria and zirconia layers.

2. Experimental

The button cells in this study had Ni–YSZ anode supports, Ni–YSZ anode functional layers, YSZ electrolytes, GDC diffusion barriers, and LSFC cathodes. All cells were prepared on anode supports containing NiO (J. T. Baker) and YSZ (Tosoh) with 1:1 weight ratio. These oxides along with Tapioca starch (10 wt%), poly(vinyl butyral) (Sigma–Aldrich, 0.5 wt%), and ethanol were mixed and ball milled for ~24 h. The resulting slurry was dried, sieved(#120 mesh) and uniaxially pressed into pellets with diameter of 19 mm. The anode support was pre-fired at 800 °C for 4 h. Colloidal solutions were deposited onto the supports to form the anode functional layer (AFL), YSZ (Tosoh) electrolyte, and the GDC (NexTech, Ohio) interlayer, respectively. The NiO-YSZ AFLs had a 1:1 weight ratio, the YSZ layers also contained 1 mol.% Fe_2O_3 (>99%, Sigma–Aldrich, UK) sintering aid, and the GDC layers had 1 mol.% Fe_2O_3 sintering aid. The resulting support/anode/electrolyte/interlayer structures were then sintered at 1250 °C or 1400 °C for 4 h, respectively. An LSCF-GDC (1:1 weight ratio) cathode functional layer (CFL) ink was screen printed onto the GDC interlayer, followed by a pure LSCF (Praxair, Washington) cathode current collector ink. The cathode layers were then fired at 1100 °C for 2 h.

Fuel cell testing was done from 650 to 800 °C with the cathode exposed to air with flow rate of 200 sccm, and the anode exposed to humidified H_2 (3 vol% H_2O) with flow rate of 100 sccm. Electrochemical impedance spectroscopy (EIS) measurements were taken on an IM6 Electrochemical Workstation (ZAHNER, Germany). The frequency range used was 100 mHz to 100 kHz with an amplitude of 20 mV.

Scanning electron microscopy (SEM, Hitachi SU8030) and electron dispersive spectroscopy (EDS, Oxford X-max 80 SDD) were used to examine cell microstructure and elemental diffusion.

After testing, cells were prepared for serial sectioning by cross sectioning, polishing and epoxy infiltration [18,19]. Imaging was done on a Zeiss Nvision 40 dual beam FIB-SEM at Argonne National Laboratory. Image segmentation and 3D reconstruction was done as described elsewhere [19]. Macrohomogeneous structural parameters such as volume percent, surface areas, triple phase boundary densities, and tortuosities were then extracted from the 3D data. Particle size distributions were defined using a 3D-volumetric method developed by Münch et al. [20].

3. Results and discussion

In order to demonstrate the advantages of the present process, cells fabricated at 1250 °C were compared directly with otherwise identical cells fired at 1400 °C. Fig. 1(a) and (b) show the voltage–current characteristics that typically result from firing at different temperatures. The 1250-fired cell yielded power density of 1.48 W cm^{-2} at 0.7 V at 800 °C, substantially higher than the 1400-fired cell – 0.94 W cm^{-2} at 0.7 V. Similar trends were observed in measurements at lower cell operating temperatures. The OCV values of the 1250-fired cells, which had Fe in the YSZ layer, were quite similar to that of the Fe-free 1400-fired cells, indicating that any electronic conductivity caused by Fe doping is negligible. The open circuit voltage (OCV) values are lower than predicted from the Nernst equation for the present fuel and oxidant compositions. For LSCF1250 cell, the OCV value measured at 800 °C is 1.060 V, compared with the predicted value of 1.10 V. However, the present cell test configuration, which utilizes Ag seals around the edges of the anode support, typically exhibits a small leakage yielding OCV values slightly lower than theoretical [21]. The mechanism of lowering sintering temperature of YSZ and GDC by the sintering aids is controversial; [22] however, liquid phase sintering is a likely mechanism. The liquid phase facilitates the rearrangement of particles in early stages of sintering, and faster dissolution-transport-precipitation process in grain boundaries. Preliminary fuel cell life tests under load for up to 546 h showed stable cell performance. More life testing is underway and will be reported elsewhere.

Fig. 1(c) and (d) present Bode and Nyquist plots of typical electrochemical impedance spectroscopy (EIS) data from the same cells as shown in Fig. 1(a) and (b). The spectra are modeled by three Cole–Cole elements in series with an inductor and resistor, $LR(RQ)(RQ)(RQ)$ with $Q = Y_o(j\omega)^n$. Only 800 °C data is shown here since the lower temperature data shows similar trends (Fig. S1 in Electronic Supplementary Information). The ohmic and polarization resistances are lower by a factor of ≥2 for the lower firing temperature, in accord with the higher P_{max} in Fig. 1(a). The ohmic resistance of the 1250-fired cell, 0.067 Ω cm^2, is as expected given the YSZ and GDC layer thicknesses and their respective conductivities: at 800 °C the 12-μm-thick YSZ layer area-specific resistance should be 0.06 Ω cm^2 and the 3-μm-thick GDC layer should be 0.0054 Ω cm^2, using a conductivity value of 0.056 S cm^{-1} [23]. This is in reasonable agreement given the range of reported conductivity values. Based on these results, the Fe doping of the electrolytes does not appear to measurably decrease the ionic conductivity. On the other hand, the ohmic resistance of the 1400-fired cell is substantially larger than expected, 0.113 Ω cm^2.

Fig. 1(c) reveals that the higher polarization resistance of the 1400 °C cell is due to increased impedance responses at ~5 and 300 Hz; such responses have previously been associated with gas diffusion and an electrochemical processes, respectively, in Ni–YSZ anodes [24–28]. Separate measurements on these cells showed that these same responses increased with decreasing hydrogen partial pressure in the fuel, verifying that they were anode responses. This suggests that the reduced firing temperature causes changes in the Ni–YSZ anode that promote both faster gas

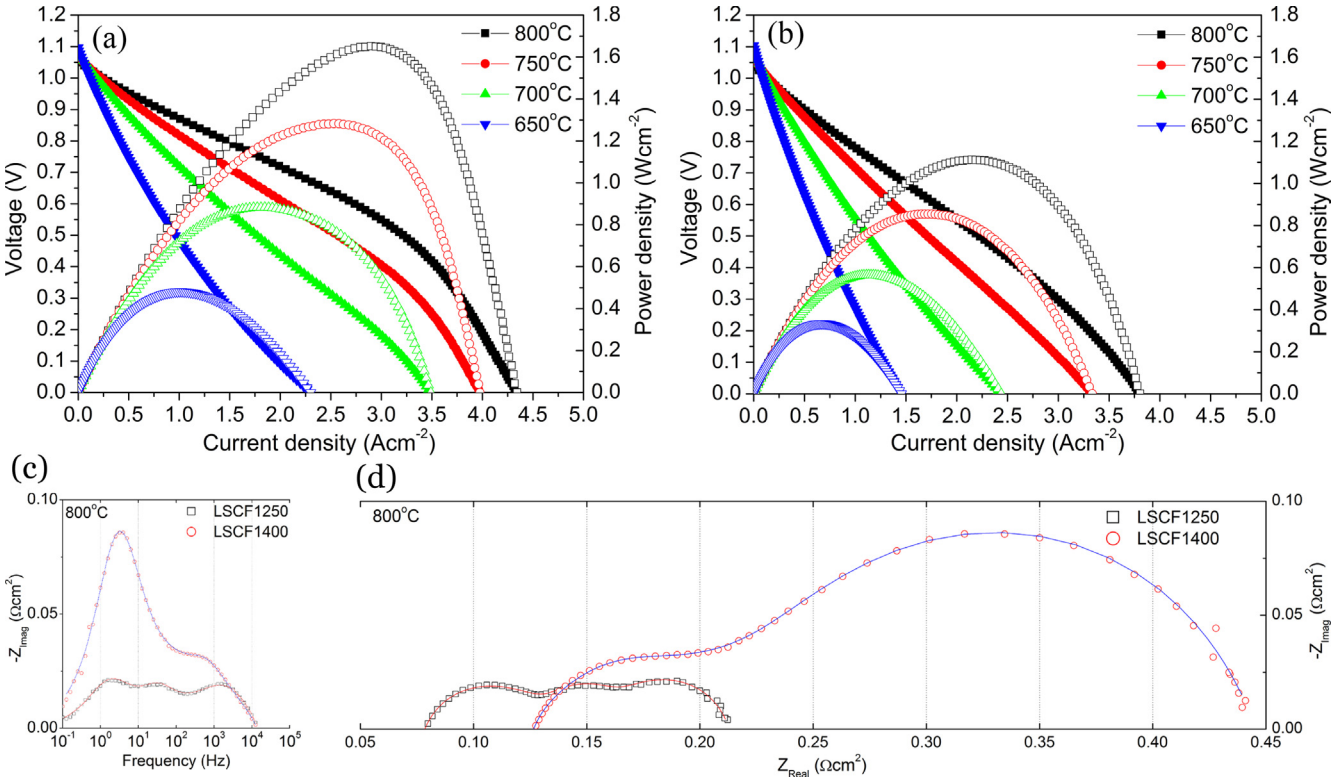

Fig. 1. Voltage and power density versus current density for button cells fired at 1250 (a) and 1400 °C (b). 1 mol.% Fe_2O_3 sintering aid was used in both cases. Bode (c) and Nyquist (d) plots of EIS data measured at 800 °C for LSCF1250 and LSCF1400 cells. The data points are measured data and the solid lines are the fits.

transport and faster electrochemical hydrogen oxidation reactions. Fig. 1(d) shows that the polarization resistance of the 1250-fired cell was much lower, 0.146 Ω cm^2, than that of the 1400-fired cell, 0.334 Ω cm^2.

Fig. 2(a) and (b) compare results of SEM measurements on cells fired at 1250 and 1400 °C. The electrodes show the expected porous structures, with no obvious difference between the cells. The 1250-fired cell showed some isolated pores in the YSZ and GDC layers, and a slightly higher density of pores at the YSZ/GDC interface. The interfacial voids probably arise from slight mismatch in the shrinkages of the two layers during firing; cells made with different Fe_2O_3 amounts in the YSZ (1 mol.% Fe_2O_3) and GDC layers (2 mol.% Fe_2O_3) showed reduced interfacial void density, presumably by better matching shrinkages. The 1400-fired cell shows fewer, but larger, pores in the YSZ layer than the 1250-fired case, while the pores at the YSZ/GDC interface also became larger and in some cases extended completely through the GDC layer.

Fig. 2(c) and (d) show SEM energy-dispersive spectroscopy line scans taken in the region near the YSZ/GDC interface. The apparent broadening of the YSZ/GDC interface in the 1250-fired cell was due in large part to the relatively low spatial resolution of energy-dispersive spectroscopy, ~1 μm. The YSZ/GDC interface was clearly broader in the 1400-fired cell, with apparent width of a few microns, consistent with prior reports [11]. These results confirm that the higher ohmic resistance of the 1400-fired cell (Fig. 2(a)) was due mainly to YSZ-GDC interdiffusion and the relatively low conductivity of the resulting solid solution [12,29], consistent with prior reports [1]. The apparent weak Sr signal in the YSZ layer of the 1400-fired cell was an artifact of peak overlaps in the EDS spectra, as shown in Fig. 2(e). That is, no Sr migration was detected in either cell, within the sensitivity of EDS, presumably due to the good diffusion barrier characteristics of the nearly dense GDC barrier layers.

The anode-related changes in cell resistance (Fig. 1(c) and (d)) were explored using three-dimensional tomography [19,30]. The tomographic data show that decreasing the firing temperature from 1400 to 1250 °C yielded decreased mean particle sizes—from 0.66 to 0.51 μm for Ni and from 0.61 to 0.45 μm for YSZ, respectively. Fig. 3 shows 3D images of the TPB lines in the anodes. The decreased temperature yielded higher active three-phase boundary (TPB) density—an increase from 3.0 to 7.2 μm^{-2} – that is explained by the smaller particle sizes [31–33]. The higher active TPB density explains the lower resistance associated with the anode electrochemical process (~300 Hz) response (Fig. 1(c)). The TPB density in the 1400-fired anode is consistent with previous results for cells fired at this temperature [19,34,35]. The 3D measurements also revealed that both anodes have only a relatively small percentage (4%) of isolated pores, so there was little impact of this on the active TPB density [19,35]. The 1250-fired cell also had a slightly higher pore volume fraction, 20.0 versus 19.2%, presumably due to reduced sintering at the lower firing temperature. This also leads to a decrease in pore tortuosity (1.89–1.81). Both these changes should increase gas diffusivity and thereby decrease concentration polarization. Although the measured structural changes seem too small to elicit the relatively large change in the ~ 5 Hz response in Fig. 1(c), it should be noted that the thick anode support also contributes substantially to the concentration polarization, and changes in this layer may be larger [30].

4. Conclusions

The present results show that the addition of Fe_2O_3 sintering aid allows reasonably dense YSZ/GDC bi-layer electrolytes to be produced by co-firing at 1250 °C, ~150 °C lower than the usual sintering temperature. The cells yielded high open-circuit voltages

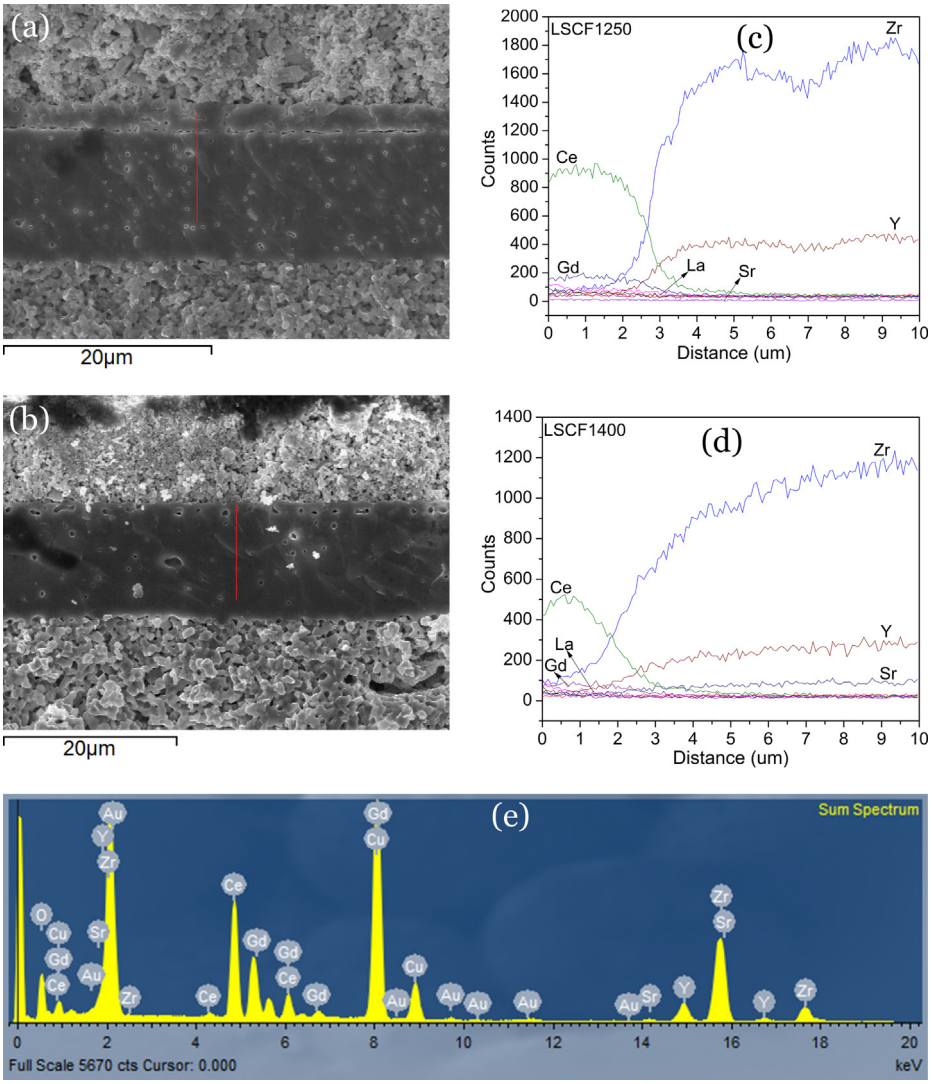

Fig. 2. Cross-sectional SEM images for LSCF1250 (a) and LSCF1400 (b) after testing. The insert red line is where the EDS line scan is taken; The intensity line scan from Gd, Ce, Zr, Y, La and Sr signals in the YSZ/GDC interface for the cell LSCF1250 (c) and LSCF1400 (d). EDS spectrum taken from the YSZ/GDC interface (e). (For interpretation of the references to color in this figure legend, the reader is referred to the web version of this article).

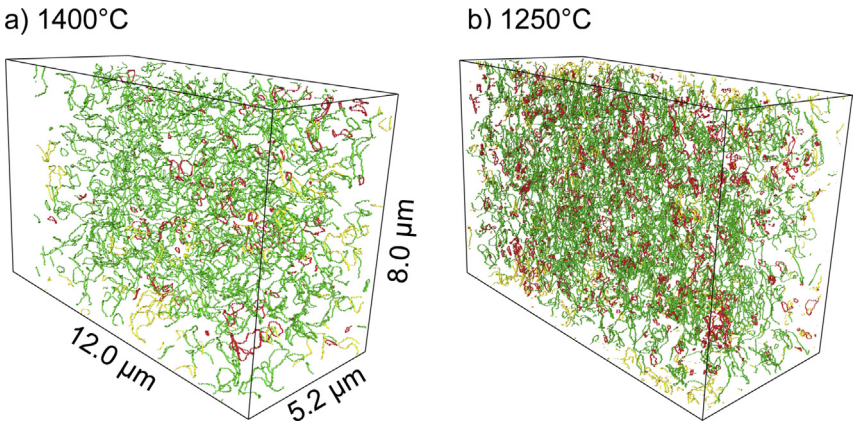

Fig. 3. FIB-SEM tomography data from the anode functional layers of the button cells fired at 1250 °C, showing the positions of TPB lines in the anode, with green indicating active, red inactive, and yellow unknown. XCT data at 1400 °C. [30]. (For interpretation of the references to color in this figure legend, the reader is referred to the web version of this article).

and the ohmic resistances were as expected given the YSZ and GDC thicknesses; suggesting that the Fe doping does not reduce ionic conductivity or cause significant electronic conductivity in the electrolyte. YSZ/GDC interdiffusion and Sr diffusion through the GDC layer were minimized. The reduced firing temperature also yielded low-polarization-resistance Ni–YSZ anodes due to a finer-scale microstructure with high TPB density and improved gas diffusion. The reduced-temperature firing process has great potential for enabling improved intermediate-temperature SOFCs by producing (1) low-resistance YSZ/GDC electrolytes that also yield high open-circuit voltage, (2) dense GDC layers that allow the use of highly-active cathode materials that are reactive with YSZ, and (3) Ni–YSZ anodes with high electrochemical activity due to fine-scale microstructure with high TPB densities.

Acknowledgment

This work is financially supported by the Global Climate and Energy Project (GCEP, grant No. 51922). The authors also gratefully acknowledge the financial support from the National Foundation Ceramics Program through Grant DMR-0907639, through which D.K. was supported to do the tomography work. The FIB-SEM was carried out in the Electron Microscopy Center for Materials Research at Argonne National Laboratory, a US Department of Energy Office of Science Laboratory operated under Contract No. DE-AC02-06CH11357 by UChicago Argonne, LLC.

Appendix A. Supplementary data

Supplementary data related to this article can be found at http://dx.doi.org/10.1016/j.jpowsour.2014.03.025.

References

[1] R. Knibbe, J. Hjelm, M. Menon, N. Pryds, M. Sogaard, H.J. Wang, K. Neufeld, J. Am. Ceram. Soc. 93 (2010) 2877–2883.
[2] S.A. Barnett, Energy 15 (1990) 1–9.
[3] T. Tsai, S.A. Barnett, Solid State Ionics 98 (1997) 191–196.
[4] T.P. Tsai, S.A. Barnett, J. Electrochem. Soc. 145 (1998) 1696–1701.
[5] E.D. Wachsman, K.T. Lee, Science 334 (2011) 935–939.
[6] Z.P. Shao, S.M. Haile, Nature 431 (2004) 170–173.
[7] T.P. Tsai, E. Perry, S. Barnett, J. Electrochem. Soc. 144 (1997) L130–L132.
[8] J.J. Bentzen, H. Schwartzbach, Solid State Ionics 40-1 (1990) 942–946.
[9] A. Mai, V.A.C. Haanappel, F. Tietz, D. Stover, Solid State Ionics 177 (2006) 2103–2107.
[10] N.M. Sammes, G.A. Tompsett, Z.H. Cai, Solid State Ionics 121 (1999) 121–125.
[11] A. Tsoga, A. Gupta, A. Naoumidis, P. Nikolopoulos, Acta Mater. 48 (2000) 4709–4714.
[12] A. Tsoga, A. Naoumidis, D. Stover, Solid State Ionics 135 (2000) 403–409.
[13] G.C. Kostogloudis, C. Ftikos, J. Eur. Ceram. Soc. 18 (1998) 1707–1710.
[14] J.A. Labrincha, F.M.B. Marques, J.R. Frade, J. Mater. Sci. 30 (1995) 2785–2792.
[15] S.P. Simner, J.P. Shelton, M.D. Anderson, J.W. Stevenson, Solid State Ionics 161 (2003) 11–18.
[16] F. Tietz, D. Sebold, A. Brisse, J. Schefold, J. Power Sources 223 (2013) 129–135.
[17] N. Jordan, W. Assenmacher, S. Uhlenbruck, V.A.C. Haanappel, H.P. Buchkremer, D. Stover, W. Mader, Solid State Ionics 179 (2008) 919–923.
[18] J.S. Cronin, K. Muangnapoh, Z. Patterson, K.J. Yakal-Kremski, V.P. Dravid, S.A. Barnett, J. Electrochem. Soc. 159 (2012) B385–B393.
[19] J.S. Cronin, J.R. Wilson, S.A. Barnett, J. Power Sources 196 (2011) 2640–2643.
[20] B. Munch, L. Holzer, J. Am. Ceram. Soc. 91 (2008) 4059–4067.
[21] D.M. Bierschenk, M.R. Pillai, Y. Lin, S.A. Barnett, Fuel Cells 10 (2010) 1129–1134.
[22] J.D. Nicholas, L.C. De Jonghe, Solid State Ionics 178 (2007) 1187–1194.
[23] V.V. Kharton, F.M. Figueiredo, L. Navarro, E.N. Naumovich, A.V. Kovalevsky, A.A. Yaremchenko, A.P. Viskup, A. Carneiro, F.M.B. Marques, J.R. Frade, J. Mater. Sci. 36 (2001) 1105–1117.
[24] R. Barfod, A. Hagen, S. Ramousse, P.V. Hendriksen, M. Mogensen, Fuel Cells 6 (2006) 141–145.
[25] S.H. Jensen, A. Hauch, P.V. Hendriksen, M. Mogensen, N. Bonanos, T. Jacobsen, J. Electrochem. Soc. 154 (2007) B1325–B1330.
[26] A. Leonide, V. Sonn, A. Weber, E. Ivers-Tiffee, J. Electrochem. Soc. 155 (2008) B36–B41.
[27] S. Primdahl, M. Mogensen, J. Electrochem. Soc. 146 (1999) 2827–2833.
[28] H.Y. Zhu, A. Kromp, A. Leonide, E. Ivers-Tiffee, O. Deutschmann, R.J. Kee, J. Electrochem. Soc. 159 (2012) F255–F266.
[29] X.D. Zhou, B. Scarfino, H.U. Anderson, Solid State Ionics 175 (2004) 19–22.
[30] D. Kennouche, Y.C.K. Chen-Wiegart, J.S. Cronin, J. Wang, S.A. Barnett, J. Electrochem. Soc. 160 (2013) F1293–F1304.
[31] J.H. Lee, H. Moon, H.W. Lee, J. Kim, J.D. Kim, K.H. Yoon, Solid State Ionics 148 (2002) 15–26.
[32] K.R. Lee, S.H. Choi, J. Kim, H.W. Lee, J.H. Lee, J. Power Sources 140 (2005) 226–234.
[33] Y. Nishida, S. Itoh, Electrochim. Acta 56 (2011) 2792–2800.
[34] J.S. Cronin, Y.C.K. Chen-Wiegart, J. Wang, S.A. Barnett, J. Power Sources 233 (2013) 174–179.
[35] J.R. Wilson, J.S. Cronin, S.A. Barnett, Scr. Mater. 65 (2011) 67–72.